RSC Advances

ROYAL SOCIETY OF CHEMISTRY

www.rsc.org/advances

Table of contents

Manuscript title： A New 12L-Hexagonal Perovskite $Cs_4Mg_3CaF_{12}$: structural transition derived from the partial substitution of Mg^{2+} with Ca^{2+}

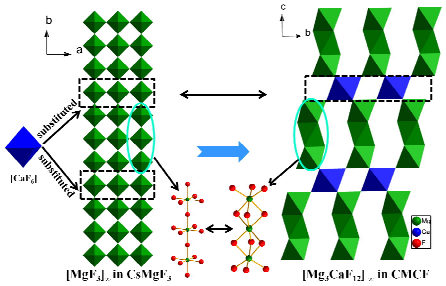

A new 12L-Hexagonal Perovskite fluoride $Cs_4Mg_3CaF_{12}$ originates from cubic $CsMgF_3$ by substituting 25% Mg^{2+} with larger Ca^{2+}. Larger Ca^{2+} extrude the space for Mg^{2+}, which lead to the structural transition.

Cite this: DOI: 10.1039/c0xx00000x

www.rsc.org/xxxxxx

Full Paper

A New 12L-Hexagonal Perovskite $Cs_4Mg_3CaF_{12}$: Structural Transition Derived from the Partial Substitution of Mg^{2+} with Ca^{2+}

Zheng Wang,[a,b] Qun Jing,[a,b] Min Zhang,*[a] Xiaoyu Dong,[a,b] Shilie Pan*[a] and Zhihua Yang[b]

Received (in XXX, XXX) Xth XXXXXXXXX 20XX, Accepted Xth XXXXXXXXX 20XX

DOI: 10.1039/b000000x

A new 12L-hexagonal perovskite $Cs_4Mg_3CaF_{12}$ was synthesized from open high-temperature solution method. It crystallizes in the trigonal space group $R\bar{3}m$ (No. 166) with lattice constants a = 6.2196(9) Å, c = 29.812(9) Å, Z = 3. $Cs_4Mg_3CaF_{12}$ is transited from cubic phase $CsMgF_3$ by replacing 25% Mg^{2+} with Ca^{2+}.The changes derived from the substitution and the structural comparison between $Cs_4Mg_3CaF_{12}$ and other perovskites are discussed in this paper. Thermal analysis, infrared spectroscopy, and electronic structure calculations were performed on the reported material.

Introduction

Fluorine has the highest electronegativity of all elements, and can combine metals to form fluorides with high chemical stability, especially for lower-electronegativity alkalis metals and alkaline earth metals. In recent years, there have been much attention paid to complex metal fluorides because of their particular physical properties such as ferromagnetic,[1] nonmagnetic insulator behavior,[2] piezoelectric characteristics,[3] and photoluminescence properties[4]. Among these important complex metal fluorides, alkali and alkaline earth metal fluorides are particularly attractive because of their applications in UV-Deep UV optical crystals, such as LiF, MF_2 (M = Mg, Ca, Ba),[5] $KMgF_3$,[6] $Li_{(1-x)}K_xBa_{(1-y)}Mg_yF_3$,[7] $NaSrF_3$, $NaBaF_3$, $LiBaF_3$,[8] $BaMgF_4$[9] crystals and so on, which can be made into high transparency and low loss optical windows, prisms, and lenses. While existed crystals cannot meet all of the application needs in UV-Deep UV wavebands. Hence, it is significant to search new fluorides used for UV-Deep UV optical materials.

Despite the simplicity of the original perovskite crystal structure, this family of compounds shows an enormous variety of structural modifications and variants. The interest in compounds belonging to this family of crystal structures arise in the large and ever surprising variety of properties exhibited and the flexibility to accommodate almost all of the elements in the periodic system. The different degrees of distortion in ABX_3 can change the perovskite symmetry from ideal cubic to rhombohedral and hexagonal.[10] In the ideal form ABX_3, the A cation is divalent, the B cation is tetravalent and X is often oxygen but also other large ions such as F^- and Cl^- are possible. In recent years, many interests have been concentrated on the mixed metal fluoride perovskites. Interestingly, in this system most of perovskites were synthesized by displacing A and partial B sites with alkali metal cations, such as Cs_2QYF_6 (Q = Na and K)[11] and Q'_2LiGaF_6 (Q' = Rb and Cs)[12]. However, if the B sites can be displaced completely by cations with other valence? We will make some efforts to answer this problem in this work.

Generally, closed environment or protective atmosphere is necessary for growing fluoride crystals because of the volatility of fluorine. Hydro/Solvent-Thermal method,[13] Bridgman-Stockbarge method[14] and Czochralski method[15] are commonly used to grow fluoride crystals, but these methods have complex processes, harsh conditions and high costs. In this paper, a new alkali-alkaline earth metallic fluoride, $Cs_4Mg_3CaF_{12}$ (CMCF), was synthesize by open high-temperature solution method. We used low-melting B_2O_3 as flux to lower the temperature of solution and decrease the volatilization of fluorine. Herein, the syntheses, crystal structure, thermal and optical properties of CMCF are presented, and the electronic structure was calculated by the first principles method to further explore the structure-property relationship.

Experimental Section

Syntheses

All commercially available chemicals (CsF, MgF_2, CaF_2 and H_3BO_3) are of reagent grade and were used as received. Small single crystals of CMCF, were grown by spontaneous crystallization with the molar ratio of CsF: MgF_2 : CaF_2 : H_3BO_3 equal to 5 : 1 : 1 : 9. A mixture of CsF (5.484 g, 36.10 mmol), MgF_2 (0.916 g, 7.35 mmol), CaF_2 (0.574 g, 7.35 mmol) and H_3BO_3 (4.540 g, 73.43 mmol) were thoroughly ground. The mixtures were then placed in a platinum crucible which was placed in a vertical, programmable-temperature furnace. The crucible were gradually heated to 800 °C and held for 30 min, then quickly cooled down to 720°C and held for 8 h, and then slowly cooled down to 650 °C at a rate of 2 °C/h, followed by rapid cooling to room temperature. Colorless crystals of CMCF were obtained, and separated mechanically from the crucible for further characterization by single-crystal XRD measurements.

Polycrystalline samples of CMCF were synthesized via

solid-state reactions. A stoichiometric mixtures of CsF, MgF_2, CaF_2 and borate acid was initially ground and placed in alumina crucibles, then heated to 720 °C under reducing atmosphere which was acquired by placing the crucible in amorphous carbon, and held for 4 days with 8 times grindings and mixings. The purity was characterized on a Bruker D2 PHASER diffractometer with Cu Kα radiation (λ = 1.5418 Å) at room temperature. The 2θ range was 10–70° with a step size of 0.02° and a fixed counting time of 1 s per step. No impurities were observed (Figure 1).

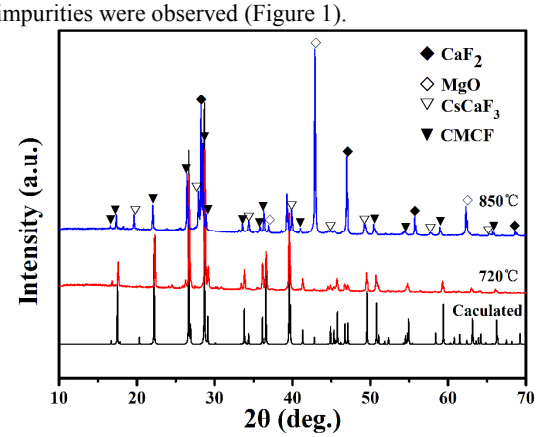

Figure 1. (a) The calculated XRD pattern (black) of CMCF derived from the single-crystal data, (b) the XRD pattern (red) of CMCF synthesized at 720 °C, (c) the XRD pattern (blue) of CMCF calcined at 850 ºC.

Single-crystal X-ray diffraction

Block crystal of CMCF (0.145 mm × 0.130 mm × 0.097 mm) were used for single-crystal data collection. Data were collected on a Bruker SMART APEX II CCD diffractometer using monochromatic Mo Kα radiation (λ = 0.71073 Å) at 293(2) K and integrated with the SAINT program.[16] The numerical absorption corrections were carried out using the SADABS program[17] for area detector. All calculations were performed with programs from the SHELXTL crystallographic software package.[18] The structure was solved by direct methods using SHELXS-97[19], and all of the atoms were refined using full-matrix least-squares techniques with anisotropic thermal parameters and final converged for I > 2σ. The structures were checked for missing symmetry elements with PLATON.[20] The crystal data and structure refinement are presented in Table 1. The selected bond distances are listed in Table S1 in the Supporting Information.The final refined atomic positions and isotropic thermal parameters are given in Table S2 in the Supporting Information.

Thermal analysis

The thermal behavior of CMCF was investigated on thermogravimetry and differential scanning calorimeter (TG-DSC) using a NETZSCH STA 449 F3 simultaneous thermal analyzer. The sample was placed in a Pt crucible and heated at a rate of 5 °C/min in the range of 40–1200 °C under flowing of nitrogen gas.

Infrared spectroscopy

An infrared spectrum ranging from 400 to 4000 cm^{-1} with a resolution of 2 cm^{-1} was recorded on a Shimadzu IR Affinity-1 Fourier transform infrared spectrometer to specify the M-F (M = Cs, Ca and Mg) bonds in CMCF. The sample was mixed thoroughly with dried KBr (5 mg of the sample and 500 mg of KBr).

Numerical Calculation Details

The electronic structure was calculated by using the DFT method implemented in the CASTEP package[21, 22]. In the present study, the cell parameters and the atomic coordinates of all the atoms were obtained from experimental values. During the calculation, the generalized gradient approximation (GGA) with Perdew-Burke-Ernzerhof (PBE) functional was adopted[23]. Under the norm-conserving pseudopotential (NCP)[24, 25], the following orbital electrons were treated as valence electrons: F $2s^2 2p^5$, Mg $2p^6 3s^2$, Ca $3s^2 3p^6 4s^2$, Cs $5s^2 5p^6 6s^1$. The kinetic energy cutoff of 940 eV was chosen, and the numerical integration of the Brillouin zone was performed using a 5 × 5 × 2 Monkhorst-Pack *k*-point sampling respectively. The other calculation parameters and convergent criteria were the default values of the CASTEP code.

Table 1 Crystal data and structure refinement for CMCF.

Empirical formula	$Cs_4Mg_3CaF_{12}$
Formula weight	872.65
Temperature (K)	296(2)
Crystal system	Trigonal
Space group, *Z*	$R\bar{3}m$, 3
a (Å)	6.2196(9)
c (Å)	29.812(9)
Volume ($Å^3$)	998.7(4)
Density (calculated, g/cm^3)	4.353
Absorption coefficient (mm^{-1})	11.512
F(000)	1152
Crystal size (mm^3)	0.145 × 0.13 × 0.097
Index ranges	$-8 \le h \le 7$, $-5 \le k \le 8$, $-38 \le l \le 37$
Reflections collected / unique	2049 / 329 [*R*(int) = 0.0183]
Completeness to theta = 27.56	99.7 %
Refinement method	Full-matrix least-squares on F^2
Data/restraints/parameters	329 / 0 / 27
Goodness-of-fit on F^2	1.202
Final *R* indices [$F_o^2 > 2\sigma(F_o^2)$][a]	*R*1 = 0.0110, *wR*2 = 0.0247
R indices (all data)[a]	*R*1 = 0.0123, *wR*2 = 0.0256
Largest diff. peak and hole ($e \cdot Å^{-3}$)	0.546 and -0.576

[a] $R1 = \Sigma||F_o| - |F_c||/\Sigma|F_o|$ and $wR2 = [\Sigma w(F_o^2 - F_c^2)^2/\Sigma wF_o^4]^{1/2}$ for $F_o^2 > 2\sigma(F_o^2)$

Results and discussion

Structural transition

Although CMCF has different space group and structure with $CsMgF_3$[26] and $CsCaF_3$[27] (parent structure), the chemical formula can also be written as $(CsMgF_3)_3 \cdot (CsCaF_3)$. Viewing from this formula, we deduce that CMCF can be regarded as 25% substitution of cubic $CsMgF_3$ with isostructural $CsCaF_3$. However, it is the difference of ionic radii between Mg^{2+} and Ca^{2+} cations that leads to the structural transition from cubic space group to trigonal space group. $CsMgF_3$ and $CsCaF_3$ are perovskite structures and crystallize in $Pm\bar{3}m$ space group. In the structure of $CsMgF_3$, [MgF_6] octahedra connect to form three dimensional (3D) frameworks by corner-sharing with Cs^+

cations inserted in void space. (Figure S1 in the Supporting Information) Mg-F bond length in $CsMgF_3$ is 2.115 Å, and Ca-F bond length in $CsCaF_3$ is 2.262 Å. When larger Ca^{2+} cations take the place of Mg^{2+} cations, there would be three changes occurred in parent structure. In order to illustrate the structural transition clearly, we choose a fragment of $CsMgF_3$ to discuss, which is shown in Figure 2.

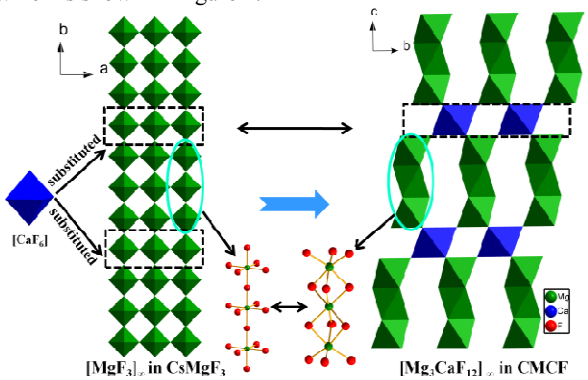

Figure 2. Structural transition from $CsMgF_3$ to CMCF.

Firstly, lager Ca^{2+} cations extrude the occupied space of $[MgF_6]$ octahedra and change the connecting mode of $[MgF_6]$ from corner-sharing to face-sharing. Three face-shared $[MgF_6]$ octahedra form an isolated $[Mg_3F_{12}]$ ***rod*** which linked into 3D framework by $[CaF_6]$ octahedra with Cs^+ cations located in void space (Figure S2 in the Supporting Information). Owing to the strain of Mg-F bonds, $[MgF_6]$ octahedra distort with bond length ranging from 1.9737(18) to 2.0660(2) Å (average: 1.9973 Å), and F-Mg-F bond angles distributing in 77.20(8)–180.0º. Besides, the coordination numbers of Cs^+ cations in CMCF and parent structures are all 12, but the Cs-F bond lengths of title compound are longer than that of parent structures.

The second change occur in $[CaF_6]$ octahedra: as shown in Figure 2, when $[CaF_6]$ octahedra replace the $[MgF_6]$ octahedra resided in dashed box, the pressure derived from different ionic radius force $[CaF_6]$ octahedra existing in isolation rather than connection. In this structure, $[CaF_6]$ octahedra play an important role which connects all of isolated ***rods***. There are also a weak distortion with F-Ca-F bond angles located in a small range: 87.27(6)–92.73(6)º (Figure S3 in the Supporting Information).

The last one is about symmetry. $CsMgF_3$ is an optical homogeneous with seven axes of the higher order (four triadaxes along <111> crystallographic direction and three tetradaxes along <100> crystallographic direction). However, the introduction of $[CaF_6]$ octahedra lower the symmetry of $CsMgF_3$ structure, which lead to trigonal space group with only one triad-rotoinversion axis along crystallographic *c* axis. (Figure 3)

Additionally, CMCF is a 12L-hexagonal perovskite which is similar to $Ba_4RR'_3O_{12}$ (R = lanthanoid and Bi, R' = Ru and Ir)[28-32]. As shown in Figure S2 in the Supporting Information, in the direction of the *c* axis, the 12L perovskite exhibits a $(cchh)_3$ sequence, where c and h correspond to corner-and face-sharing octahedra, respectively. In general, reported examples of metal fluoride hexagonal perovskites appear to have an $A'_2BB'F_6$ composition, such as K_2LiAlF_6, Rb_2LiGaF_6,[12a] Cs_2NaFeF_6, Cs_2NaCrF_6,[12b] and Cs_2NaNiF_6[33]. However, the title compound has another composition $A'_2B'_{1.5}B''_{0.5}F_6$, which derives from ABX_3 perovskite by replacing the A and B sites with alkali metal, and alkaline earth metal cations, respectively.

In order to characterize the degree of distortion for CMCF, tolerance factor ($t = (r_A + r_X)/\sqrt{2}\,(r_B + r_X)$) was calculated, which equal to 1.07. For comparison, the tolerance factor *t* for $CsMgF_3$ and $CsCaF_3$ are also obtained, which are 1.13[34] and 0.94[35], respectively. Viewing from this, it is curious that $CsMgF_3$ with high tolerance factor adopts a cubic structure[36] and a large difference exists between the two isostructural parent structures. The different ratio of ionic radii between A and B cations should be responsible for these. As we can see from the Figure S4 in the Supporting Information, it is suitable for Cs^+ cations fitting into the interstices of adjacent $[CaF_6]$ octahedra, which brings an ideal cubic perovskite with $t = 0.94$. However, Cs^+ cations are too large to fit into the interstices of $[MgF_6]$ octahedral, thus resulting in a higher tolerance factor 1.13. For CMCF, inclusion of larger Ca^{2+} cations can relieve the tension caused by too much face-sharing $[MgF_6]$; and decrease the contradiction brought by too large A cations versus too small B cations, which lead to $t = 1.07$.

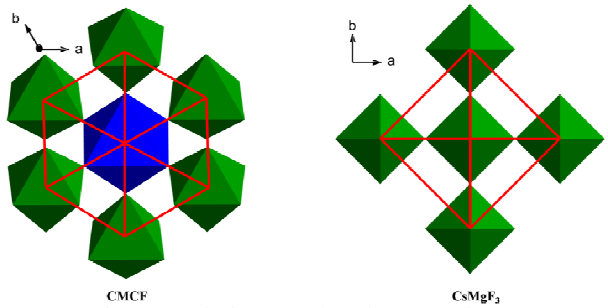

Figure 3. The symmetrical comparation of CMCF and $CsMgF_3$ (green octahedra are $[MgF_6]$ octahedra and blue one is $[CaF_6]$ octahedron).

Thermal analysis

Viewing from the TG-DSC curves of CMCF (Figure 4), the title compound only appear one clear endothermic peak at 795 ºC, and corresponding with obvious weight loss, which tentatively suggests that title compound melt incongruently. In order to assign the endothermic peak, the samples of CMCF were calcined at 850 ºC for 10 h. As shown in Figure 1, CMCF are partially decomposed into MgF_2 which is oxidize into MgO (JCPDS No. 45-0946), CaF_2 (JCPDS No. 35-0816) and $CsCaF_3$ (JCPDS No. 28-0817) with the volatilization of Cs and F elements; Hence, the endothermic peak are the decomposed peaks of CMCF.

Infrared spectroscopy

To trace the Cs-F, Mg-F and Ca-F bonds in CMCF, the infrared spectrum measurement was performed. Figure S5 shows the complete spectral region of the infrared spectrum between 400 and 4000 cm^{-1}. Only one sharp peak located 448 cm^{-1} is observed. Referring to the literature[37], this peak is the characteristic peak of metallic-fluorine bond. The infrared spectrum further confirms the existence of M-F bonds (Cs-F, Mg-F or Ca-F), consistent with the results obtained from the single-crystal X-ray structural analyses.

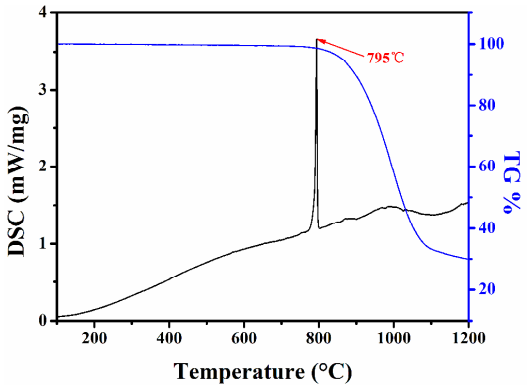

Figure 4. TG-DSC curves of CMCF.

Electronic structures

Electronic structure calculations were performed in order to examine their band structures and explain the relationships between electronic structures and optical properties. The electronic structures of CMCF were determined using the plane-wave pseudopotential calculations. The calculated band structure of CMCF along high symmetry points of the first Brillouin zone are plotted in Figure S6 in the Supporting Information. It is found that the lowest energy of the conduction bands (CBs) is localized at the G point, whereas the highest of the valence bands (VBs) is localized at the G point with a band gap of 7.10 eV. Therefore, CMCF is a direct bandgap insulator.

As seen from the total and partial densities of states (TDOS, PDOS) analyses of CMCF (Figure 5), the VBs below the Fermi level are derived from F 2*p* orbitals, Cs 5*p* and 6*s* orbitals, Mg 2*p* and 3*s* orbitals and Ca 3*p* and 4*s* orbitals. While, the CBs above the Fermi level are derived from Cs 5*p* and 6*s* orbitals, Mg 2*p* and 3*s* orbitals, Ca 3*p* and 4*s* orbitals and F 2*s* and 2*p* orbitals. One can see that VBs are mostly determined by F 2*p* orbitals, the contribution of Cs 5*p*, Mg 3*s*, Mg 2*p*, Cs 6*s*, Ca 3*p* and Ca 4*s* orbitals decrease progressively; and for CBs, the *p* orbital of every element contributes more than its *s* orbital.

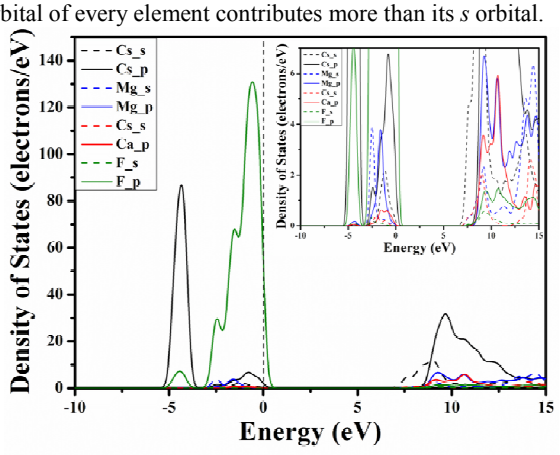

Figure 5. Total DOS and partial DOS of CMCF.

Additionally, the charge density of CMCF is presented in Figure S7 in the Supporting Information. Viewing from this figure, we find that electrons gather around the ***rods***, which intuitively shows the existence of extruding force brought by lager Ca^{2+} cations.

Conclusions

A new 12L-hexagonal perovskite alkali and alkaline earth metal mixed fluoride $Cs_4Mg_3CaF_{12}$ was reported. The title compound can be regarded as the partial substitution of two parent structures (isostructural cubic $CsMgF_3$ and $CsCaF_3$). Larger Ca^{2+} cations taking the place of Mg^{2+} cations can change the connection mode from corner-sharng to face-sharing; make $[CaF_6]$ octahedra existed in isolation rather than connection; and decrease the number of parent structural axes of the higher order from seven to one to lower the symmetry of parent structure. The charge density intuitively shows the existence of extruding force brought by lager Ca^{2+} cations. The $Cs_4Mg_3CaF_{12}$ belongs to a new hexagonal perovskite composition $A'_2B'_{1.5}B''_{0.5}F_6$, which derives form replacing A and B sites of cubic ABX_3 perovskite with alkali metal Cs^+ cations, and alkaline earth metal Mg^{2+} and Ca^{2+} cations. Further research on this compound is underway.

Acknowledgments

This work is supported by Western Light of CAS (Grant No. XBBS201217), 973 Program of China (Grant No. 2012CB626803), the National Natural Science Foundation of China (Grant Nos. U1129301, 51172277, 21101168, 11104344), Main Direction Program of Knowledge Innovation of CAS (Grant No. KJCX2-EW-H03-03), The Funds for Creative Cross & Cooperation Teams of CAS, Major Program of Xinjiang Uygur Autonomous Region of China during the 12th Five-Year Plan Period (Grant No. 201130111), the High Technology Research & Development Program of Xinjiang Uygur Autonomous Region of China (Grant No. 201116143), the Science and Technology Project of Urumqi (Grant No. G121130002).

Notes and references

[a] *Key Laboratory of Functional Materials and Devices for Special Environments of CAS; Xinjiang Key Laboratory of Electronic Information Materials and Devices; Xinjiang Technical Institute of Physics & Chemistry of CAS, 40-1 South Beijing Road, Urumqi 830011, China*
[b] [b]*University of Chinese Academy of Sciences, Beijing 100049, China*

† Electronic Supplementary Information (ESI) available: [atomic coordinates and equivalent isotropic displacement parameters, structure of cubic $CsMF_3$ (M = Mg and Ca), crystal structure of CMCF, bond angles of $[CaF_6]$ octahedra, IR spectrum, band structure and charge density]. See DOI: 10.1039/b000000x/

1 A. H. Cooke, D. A. Jones, J. F. A. Silva and M. R. Weils, *J. Phys. C.: Solid State Phys.*, 1975, **8**, 4083.
2 R. A. Heaton and C. Lin, *Phys. Rev., B*, 1982, **25**, 3538.
3 M. Eibschutz and H. J. Guggenheim, *Solid State Commun.*, 1968, **6**, 737.
4 (a) D. K. Sardar, W. A. Sibley and R. Aicala, *J. Lumin.*, 1982, **27**, 401; (b) A. Gektin, I. Krasovitskaya and N. Shiran, *J. Lumin.*, 1997, **664**, 72.
5 N. G. Gerasimova, *Instrum. Exp. Tech.* 2006, **49**, 408.
6 (a) M. Sahnoun, M. Zbiri, C. Daul, R. Khenata, H. Baltache and M. Driz, *Mater. Chem. Phys.*, 2005, **91**, 185; (b) M. Yanagihara, M. Zamri Yusop, M. Tanemura, S. Ono, T. Nagami, K. Fukuda, T. Suyama, Y. Yokota, T Yanagida and A. Yoshikawa, *APL Mater.*, 2014, **2**, 046110.
7 R. E. Ouenzerfi, S. Ono, A. Quema, M. Goto, M. Sakai and N.Sarukura, *J. Appl. Phys.*, 2004, **96**, 7655.
8 Y. Oyama, *Optical member for vacuum ultraviolet, and aligner and device manufacture method using same*, United States, US6813070.
9 (a) L. Mateos, M. O. Ramírez, I. Carrasco, P. Molina, J. F. Galisteo-López, E. G. Víllora, C. Heras, K. Shimamura, C. Lopez and L. E.

Bausá, *Adv. Funct. Mater.*, 2014, **24**, 1509; (b) L. L. Kang, T. Y. Liu, Q. R. Zhang, L. Z. Xu and F. W. Zhang, *Chin. Phys. B*, 2011, **20**, 047101.
10 (a) A. S. Bhalla, R. Guo and R. Roy, *Mat. Res. Innovat.*, 2000, **4**, 3; (b) M. R. Levy, *Crystal Structure and Defect Property Predictions in Ceramic Materials*, Imperial College, 2005, ch.3, pp. 79-144.; (c) N. L. Allan, M. J. Dayer, D. T. Kulp, and W. C. Mackrodt, *J. Mater. Chem.*, 1991, **1**, 1035.
11 A. Vedrine, J. P. Besse, G. Baud, M. Capestan, Rev. Chim. Miner., 1970, 7, 593.
12 (a) J. Graulich, S. Drueeke and D. Babel, *Z. Anorg. Allg. Chem.*, 1998, **624**, 1460; (b) D. Babel, and R. Haegele, *J. Solid State Chem.*, 1976, **18**, 39.
13 (a) L. N. Demianets, *Prog. Crystal Growth and Charact.*, 1990, **21**, 293.; (b) C. Y. Zhao, S. H. Feng, Z. C. Zhao, C. S. Shi, R, R. Xu and J. Z. Ni, *Chem. Commun.*, 1996, **14**, 1641.
14 K. Recker, F. Wallrafen, and S. Haussühl, *J. Cryst. Growth*, 1974, **26**, 97.
15 (a) J. Y. Lin, Y. F. Ruan, J. Wang, J. Liu and B. X. Huan, *J. Rare Earth.*, 2004, **22**, 126; (b) K. Shimamura, E. G. Villora, K. Muramatsu, and N. Ichinose, *J. Cryst. Growth*, 2005, **275**, 128.
16 *SAINT: Program for Area Detector Absorption Correction, Version 4.05*; Siemens Analytical X-ray Instruments: Madison, WI, 1995.
17 R. H. Blessing, *Acta Crystallogr. Sect. A*, 1995, **51**, 33.
18 G. M. Sheldrick, *SHELXTL, version 6.12*, Bruker Analytical Xray Instruments, Inc.: Madison, WI, 2001.
19 G. M. Sheldrick, *SHELXS-97, Program for X-ray Crystal Structure Solution*, University of Göttingen, Göttingen, Germany, 1997.
20 L. J. Spek, *Appl. Crystallogr.*, 2003, **36**, 7.
21 S. J. Clark, M. D. Segall, C. J. Pickard, P. J. Hasnip, M. J. Probert, K. Refson and M. C. Payne, Z. Kristallog., 2005, **220**, 567.
22 B. G. Pfrommer, M. Cote, S. G. Louie and M. L. Cohen, *J. Comput. Phys.* 1997, **131**, 233.
23 J. P. Perdew, K. Burke and M. Ernzerhof, *Phys. Rev. Lett.*, 1996, **77**, 3865.
24 A. Rappe, K. Rabe, E. Kaxiras and J. Joannopoulos, *Phys. Rev. B*, 1990, **41**, 1227.
25 J. Lin, A. Qteish, M. Payne and V. Heine, *Phys. Rev. B*, 1993, **47**, 4174.
26 G. Q. Wu and R. Hoppe, *Z. Anorg. Allg. Chem.*, 1984, **514**, 92.
27 W. L. W. Ludekens, A. J. E. Welch, Acta Cryst., 1952, 5, 841–841.
28 Y. Shimoda, Y. Doi, Y. Hinatsu and K. Ohoyama, *Chem. Mater.*, 2008, **20**, 4512.
29 Y. Shimoda, Y. Doi, M. Wakeshima and Y. Hinatsu, *J. Solid State Chem.*, 2009, **182**, 2873.
30 Y. Shimoda, Y. Doi, M. Wakeshima and Y. Hinatsu, *Inorg. Chem.*, 2009, **48**, 9952.
31 Y. Shimoda, Y. Doi, M. Wakeshima and Y. Hinatsu, *J. Solid State Chem.*, 2010, **183**, 33.
32 W. Miiller, M. T. Dunstan, Z. X. Huang, Z. Mohamed, B. J. Kennedy, M. Avdeev and C. D. Ling, *Inorg. Chem.*, 2013, **52**, 12461.
33 E. Alter and R. Hoppe, *Z. Anorg. Allg. Chem.*, 1974, **405**, 167.
34 W. L. W. Ludekens and A. J. E. Welch, *Acta Cryst.*, 1952, ***5,*** 841.
35 M. H. Jo, H. H. Park, C. H. Kim and K. S. Suh, *J. Mater. Sci. Lett.*, 1996, **15**, 1294.
36 M. Johnsson and P. Lemmens, *Crystallography and Chemistry of Perovskites*, in *Handbook of Magnetism and Advanced Magnetic Materials*, ed. H. Kronmüller and S. Parkin, John Wiley & Sons Ltd, Chichester, 2006, Vol. 4, Uk, pp. 2098-2106.
37 K. Nakamoto, *Infrared and Raman Spectra of Inorganic and Coordination Compounds Part B: Applications in Coordination, Organometallic, and Bioinorganic Chemistry*, Sixth edition, John Wiley & Sons, Hoboken, 2009, 193–198.